Check for updates

Advanced Electronic Materials

ADVANCED ELECTRONIC MATERIALS Open Access

www.advelectronicmat.de

RESEARCH ARTICLE OPEN ACCESS

Lateral Profile of Doping Concentration Extracted From the C-V Characteristics in Self-Aligned Top-Gate Coplanar InGaZnO Thin-Film Transistors

Seung Joo Myoung[1] | Chang Il Ryoo[2] | Jingyu Park[1] | Dong Hyeop Shin[1] | Su Han Noh[1] | Sae Him Jung[1] | Soohong Eo[1] | Wonjung Kim[1] | Sung Jun Yun[2] | Jae Moon Soh[2] | Yoo Seok Park[2] | Changwook Kim[1] | Dong Myong Kim[1] | Sung-Jin Choi[1] | Yoon Jung Lee[1] | Ickhyun Song[3] | Dae Hwan Kim[1]

[1]School of Electrical Engineering, Kookmin University, Seoul, Republic of Korea | [2]Large Display Business Unit, LG Display Company, Paju, Republic of Korea | [3]Department of Electronic Engineering, Hanyang University, Seoul, Republic of Korea

Correspondence: Ickhyun Song (isong@hanyang.ac.kr) | Dae Hwan Kim (drlife@kookmin.ac.kr)

Received: 20 November 2025 | **Revised:** 3 March 2026 | **Accepted:** 10 April 2026

Keywords: amorphous InGaZoO (a-IGZO) | capacitor-voltage (C-V) method | later-doping profile | thin-film transistor (TFT) | threshold voltage (V_T) roll-off

ABSTRACT

Self-aligned top-gate (SATG) amorphous InGaZnO (a-IGZO) thin-film transistors (TFTs) are strong candidates for low-power display backplanes and back-end-of-line (BEOL)-integrated circuits. Their scaling, however, is limited by short-channel effects (SCEs), such as threshold-voltage (V_T) roll-off and drain-induced barrier lowering (DIBL), which are strongly influenced by the lateral effective doping profile, $N_D(y)$, formed by oxygen-vacancy/hydrogen-related donor diffusion from the source/drain (S/D) extensions. Conventional transfer length method (TLM) approaches provide only indirect, lumped estimates and often lose accuracy in low-doping regions. Here, we propose a capacitance–voltage (C–V)-based extraction technique that directly reconstructs $N_D(y)$ and key profile parameters—including overlap length (L_{OV}), gradient length (L_{Grad}), and base doping concentration ($N_{D,Base}$)—from measured gate capacitances ($C_{GG}/C_{GS}/C_{GD}$). Using L-split SATG a-IGZO TFTs with channel lengths ranging from 4.5 to 40 μm, we validate the extracted profiles by directly comparing them with those obtained from a TLM-based extraction and demonstrate the quantitative prediction of V_T (V_{ON}) roll-off across different channel lengths. The results reveal that S/D dopant overlap increases the channel -center doping $N_{D,ch}$ in short channels, thereby accelerating V_T roll-off and enhancing DIBL. This C–V-based lateral profiling framework provides practical diagnostics and design guidelines for suppressing SCEs in future low-power, high-reliability oxide electronics.

1 | Introduction

Oxide thin-film transistors (TFTs) have attracted considerable attention as key devices for next-generation display technologies and back-end-of-line (BEOL) integrated circuits, owing to their advantages such as process compatibility at low temperatures, transparency with electrode materials, and excellent uniformity in large area [1–3]. Among them, amorphous indium–gallium–zinc oxide (a-IGZO) has emerged as a promising candidate for high-resolution and high-refresh-rate displays as well as low-power integrated circuits, due to its high field-effect mobility and excellent reliability [4–6]. However, there exists a critical

Seung Joo Myoung and Chang Il Ryoo contributed equally to this work.

This is an open access article under the terms of the Creative Commons Attribution License, which permits use, distribution and reproduction in any medium, provided the original work is properly cited.

© 2026 The Author(s). *Advanced Electronic Materials* published by Wiley-VCH GmbH

challenge of short-channel effects (SCEs) that arise as the device technology scales. Representative SCEs include the channel-length dependence of the threshold voltage (i.e., V_T roll-off) and its drain voltage dependence (or drain-induced barrier lowering, DIBL), both of which are strongly affected by the magnitude and distribution of the effective doping concentration within the channel [7, 8].

Unlike Si MOSFETs, where lateral doping is intentionally engineered by lightly doped drain (LDD) structures, oxide TFTs inherently suffer from uncontrolled dopant diffusion, such as oxygen vacancies (V_O) and hydrogen (H), from the source/drain regions into the channel [9]. This fundamental difference highlights the necessity of precise characterization and engineering of lateral doping profile to enable further oxide TFT scaling. In particular, self-aligned top-gate (SATG) coplanar IGZO TFTs are highly vulnerable to non-uniform lateral doping profiles induced by V_O/H diffusion from the n^+ source/drain extensions, which can cause V_T roll-off even at channel lengths of several micrometers [10].

The conventional transfer-length method (TLM) has been widely used to extract doping-related parameters, where series resistance analysis provides indirect estimates of the effective channel length (L_{eff}) and carrier distribution [11, 12]. In oxide TFTs, however, strong dependence of field-effect mobility and trap-limited transport characteristics on the gate bias introduces significant errors in doping estimation [13]. Moreover, TLM inherently yields only lumped resistance values, and thus, it often fails to resolve channel-length-dependent variations of individual doping profiles. In this respect, to achieve a quantitative analysis and reliable prediction of SCEs in oxide TFTs, a new approach that can directly extract $N_D(y)$ with higher channel-length resolution is indispensable.

In this study, we propose a new extraction technique for lateral doping profile based on capacitance–voltage (C–V) characteristics in order to overcome the potential limitations of conventional methods. The proposed approach quantitatively derives the position-dependent doping concentration $N_D(y)$ by analyzing the variation of the accumulation area with gate bias. Furthermore, key parameters defining $N_D(y)$, such as the overlap length (L_{OV}), the gradient region length (L_{GRAD}), the base region length (L_{BASE}), and the doping gradient (σ), can be directly extracted from experiments. These parameters enable precise identification of the origins of SCEs, including V_T roll-off and DIBL. The validity of the proposed method is established through a fully experimental verification framework using L-split SATG a-IGZO TFTs. Specifically, the extracted $N_D(y)$ is directly compared with a TLM-based extraction, and the profiles are further used to quantitatively predict $V_T(V_{ON})$ roll-off across channel lengths. This method not only overcomes the inherent limitations of the conventional methods but also offers practical design guidelines for suppressing SCEs in BEOL-compatible low-power devices and next-generation display driver circuits.

2 | Experimental Section

In this work, self-aligned top-gate (SATG) a-IGZO TFTs were fabricated. A 30-nm-thick a-IGZO active layer (In:Ga:Zn = 1:1:1 at%) was deposited by DC-magnetron sputtering. A 100 nm-thick SiO_2 gate dielectric was subsequently deposited by plasma-enhanced chemical vapor deposition (PECVD). After deposition of the gate electrode, the gate/dielectric stack was patterned simultaneously, with wet etching for the metal and dry etching for the dielectric. The n^+ source/drain regions were formed by inducing oxygen vacancies through plasma treatment after gate dielectric etching. Due to the different etch selectivity of the gate and dielectric layers, the gate edge and n^+ doping boundary were not perfectly aligned, leading to a finite offset position (y_0). The fabricated devices had a channel width (W) of 50 μm and channel lengths (L) ranging from 4.5 to 40 μm. Electrical characteristics were measured using a semiconductor parameter analyzer (Agilent 4156C). Capacitance–voltage (C–V) measurements were carried out at 100 kHz, using a precision LCR meter (HP 4284A). The list of key parameters and their definitions used in this study are summarized in Table 1.

2.1 | C–V Method for N_D Profile Extraction

Figure 1 illustrates the basic concept of the proposed C–V based lateral doping profile extraction method. Figure 1a shows a schematic cross-section of a self-aligned top-gate (SATG) coplanar oxide TFT and the variations of the accumulation area in the channel as the gate voltage (V_G) changes between the minimum capacitance voltage ($V_{G,min}$) and the turn-on voltage (V_{ON}). (The detailed definitions of $V_{G,min}$ and V_{ON} are provided later.) In this structure, the lateral doping profile is inherently non-uniform due to V_O/H diffusion from the n^+ source/drain extensions [14]. As V_G decreases below V_{ON}, de-accumulation (i.e., electron depletion from the accumulated state, not inversion) starts from the channel center—where the doping concentration is the lowest—and the accumulation area progressively shrinks toward the S/D regions. This behavior arises from the non-uniform lateral $N_D(y)$: the channel center typically has the lowest effective doping (or equilibrium carrier density) and therefore loses accumulation first as V_G is reduced. Figure 1b shows the variation of the gate capacitance as a function of gate voltage. C_{GG} is measured by applying an AC signal to the gate while tying the source and drain together, whereas C_{GD} and C_{GS} are measured between the gate–drain and gate–source terminals, respectively. By comparing C_{GD} and C_{GS}, the lateral doping distributions near the source and drain sides can be independently characterized. The measurements were performed using a precision LCR meter (HP 4284A) at an AC frequency of 100 kHz. C_{para} represents the parasitic capacitance associated with the pads and interconnections. Figure 1c illustrates the schematic definition of the key parameters related to the channel doping distribution. From the C_{GG} value at a given gate voltage V_1, the onset position of accumulation (y_1) can be identified, which can then be correlated with the turn-on voltage distribution to derive the spatial doping concentration $N_D(y)$. L_{OV} denotes the overlap region where the doping concentration exceeds the critical value N_C, forming a metallic n^+ extension that contributes a gate-voltage-independent capacitance. L_{Grad} corresponds to the transition region with a gradual change in doping, reflected as variations in the accumulation area and C–V response. L_{Base} represents the base channel region that retains a uniform doping concentration $N_{D,ch}$ near the channel center. The principle of the proposed method is as follows. As the gate voltage decreases below V_{ON}, de-accumulation (electron

2199160x, 2026, 10, Downloaded from https://advanced.onlinelibrary.wiley.com/doi/10.1002/aelm.202500841 by Hanyang University Library, Wiley Online Library on [19/11/2026]. See the Terms and Conditions (https://onlinelibrary.wiley.com/terms-and-conditions) on Wiley Online Library for rules of use; OA articles are governed by the applicable Creative Commons License

TABLE 1 | Summary of key parameters and descriptions used in this study.

Parameters [units]	Description
L_{eff} (μm)	Effective channel length
L_{Gate} (μm)	Gate length
L_{OV} (μm)	Gate-n^+ overlap length
L_{Grad} (μm)	length of area where N_D changes
L_{Base} (μm)	Length of area where N_D equals base doping concentration
y_0 (μm)	n^+ doping edge position
l_0 (μm)	Characteristic length of dopant diffusion profile
σ (μm/decade)	Doping gradient
$N_{D,n+}$ (cm^{-3})	Doping density of n^+ region
$N_{D,Base}$ (cm^{-3})	Base doping density of the channel
$N_{D,ch,\ n+\ OVL}$ (cm^{-3})	Diffused dopant density of channel from n^+ region
$N_{D,ch}$ (cm^{-3})	Doping density of the channel center ($N_{D,Base} + N_{D,ch,\ n+OVL}$)
$V_{G,min}$ (V)	Minimum capacitance voltage
V_{ON} (V)	Turn-on voltage
C_{GG} (F)	Gate capacitance measured to the gate while tying the source and drain together
C_{GD} (F)	Gate capacitance measured between the gate–drain terminals
C_{GS} (F)	Gate capacitance measured between the gate–source terminals
C_{para} (F)	Parasitic capacitance
$n_0(y)$ (cm^{-3})	the equilibrium carrier concentration profile
$N_D(y)$ (cm^{-3})	lateral-doping profile
$\Delta N_{D,Base}(L)$ (cm^{-3})	Base doping variation with channel length

depletion from the accumulated state) initiates from the channel center with the lowest doping concentration. Consequently, the accumulation area progressively shrinks and the measured gate capacitance decreases. For clarity, the term 'de-accumulation' here refers to the reduction of accumulated electron density in an accumulation-mode oxide TFT, rather than the formation of an inversion layer. By mapping the capacitance value at a given V_G (V_1) to its corresponding onset position (y_1), the lateral doping concentration $N_D(y_1)$ can be directly reconstructed.

Figure 2 illustrates the step-by-step procedure of the proposed lateral-doping extraction method based on C–V measurement. Figure 2a defines the voltage range used for analyzing the n_0 and N_D profiles from the C–V characteristics. The analysis window is set between the minimum capacitance point ($V_{G,min}$), where C_{GDS} begins to saturate, and the turn-on voltage (V_{ON}), defined as the V_G at which C_{GG}–$C_{GS(D)}$ reaches its maximum in the C–V curve. This V_{ON} coincides with the turn-on voltage extracted from the transfer curve at $I_{DS} = W/L \times 10^{-11}$ A. Below $V_{G,min}$, y_1 does not vary and n_0 continuously increases, while beyond V_{ON} the entire channel is in accumulation, preventing spatial extraction of $N_D(y)$.

In addition, several key electrical parameters can also be obtained from the C–V curves. To specify this definition, parasitic capacitance (C_{para}) is the difference between the minimum $C_{GS(D)}$ and the minimum of C_{GG}–$C_{GS(D)}$. The gate-oxide capacitance per unit area (C_{OX}) is given by (max C_{GG} – C_{para})/(W·L_{Gate}). The effective channel length (L_{eff}) is calculated as (max C_{GG} – min C_{GG})/(C_{OX}·W). The overlap length (L_{OV}), corresponding to the metallic n^+ region where $N_D \geq N_C$, is extracted at $V_{G,min}$ using (min C_{GG} – min C_{GD}) = C_{OX}·W·L_{OV}, or alternatively from the regression of $N_D(y)$ at $N_D = N_C$ ($\approx 5.0 \times 10^{18}$ cm^{-3}). The expression (min C_{GG} – min C_{GD}) = C_{OX}·W·L_{OV} corresponds to the symmetric-overlap case where $L_{OV,S} \approx L_{OV,D}$. Here, C_{GG} at $V_{G,min}$ contains the overlap contributions from both sides, whereas C_{GS} and C_{GD} mainly include the source-side and drain-side overlap contributions, respectively. Therefore, potential source/drain asymmetry can be explicitly addressed by extracting $L_{OV,S}$ = (min C_{GG} – min C_{GD})/(C_{OX}·W) and $L_{OV,D}$ = (min C_{GG} – min C_{GS})/(C_{OX}·W). In this work, L_{OV} is defined as $L_{OV} \equiv (L_{OV,S} + L_{OV,D})/2$, because $L_{OV,S}$ and $L_{OV,D}$ were found to be comparable within the experimental uncertainty. For devices with pronounced asymmetry,

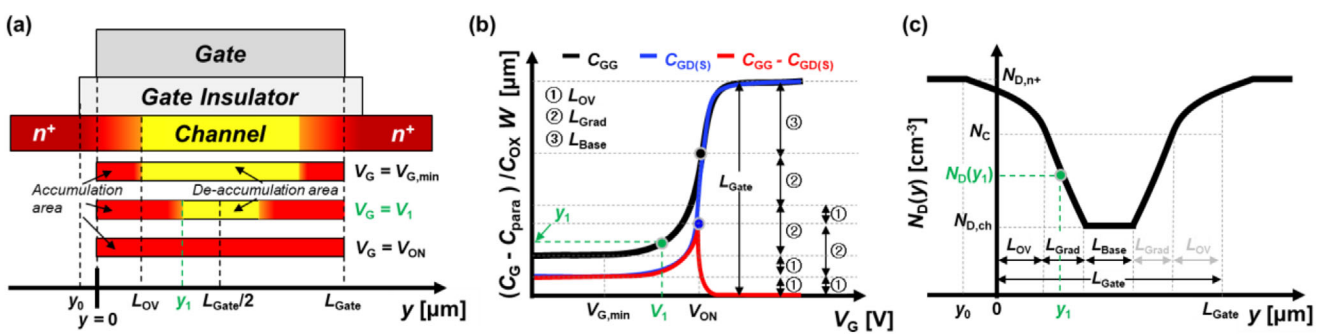

FIGURE 1 | a) Cross-sectional structure of a SATG a-IGZO TFT and the variation of the accumulation area as V_G is swept from $V_{G,min}$ to V_{ON}. b) Gate capacitances C_{GG}, C_{GD}, and C_{GS} measured at 100 kHz. It shows independent extraction results of source- and drain-side doping. C_{para} denotes parasitic capacitance. c) The schematic of doping concentration distribution ($N_D(y)$) and graphical definition of key parameters in $N_D(y)$, including L_{OV}, L_{Grad}, and L_{Base}.

2199160x, 2026, 10, Downloaded from https://advanced.onlinelibrary.wiley.com/doi/10.1002/aelm.202500841 by Hanyang University Library, Wiley Online Library on [19/11/2026]. See the Terms and Conditions (https://onlinelibrary.wiley.com/terms-and-conditions) on Wiley Online Library for rules of use; OA articles are governed by the applicable Creative Commons License

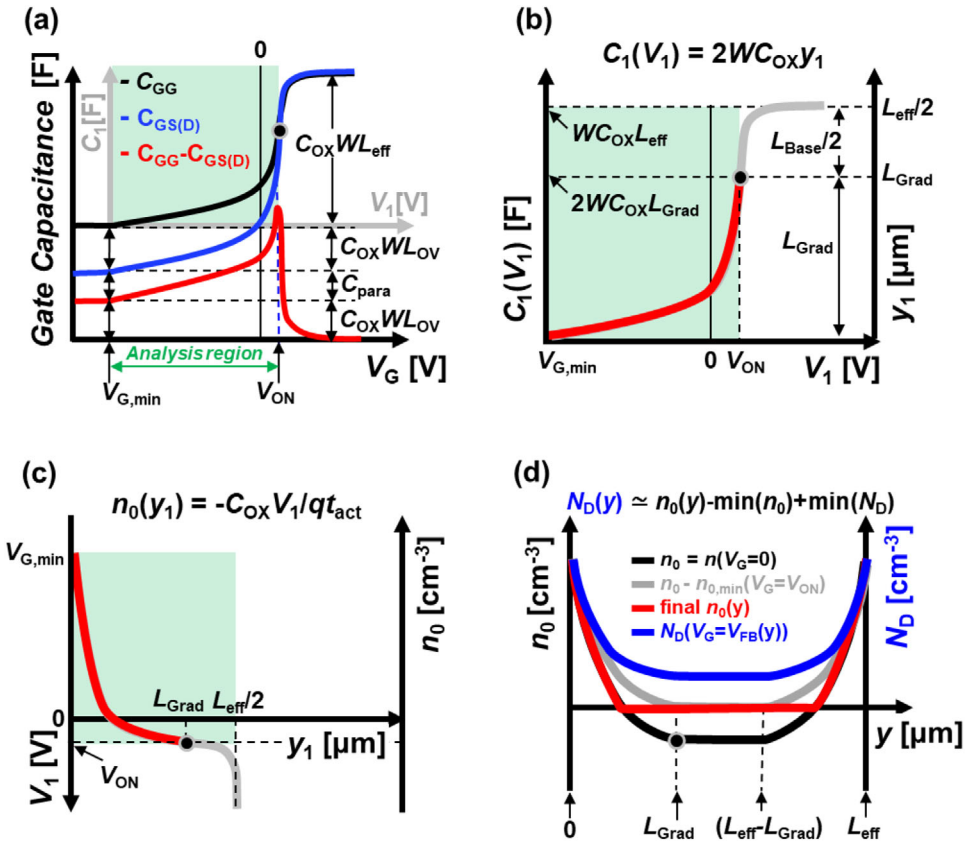

FIGURE 2 | Step-by-step procedure for extracting $N_D(y)$ from C–V measurement. a) Voltage window defined between $V_{G,min}$ and V_{ON} for valid analysis. b) Relation between capacitance increment C_1 and the accumulation onset position y_1. c) Conversion of $V_1(y_1)$ into the equilibrium carrier distribution $n_0(y)$ via integration of the incremental capacitance C_1 from V_1 to 0 V. d) Construction of $n_0(y)$ and conversion into $N_D(y)$ profile.

the subsequent relations can be generalized by replacing $2L_{OV}$ with $L_{OV,S} + L_{OV,D}$. The gradient length (L_{Grad}) is obtained as $C_1(V_{ON})/(2W{\cdot}C_{OX})$, and the base channel length (L_{Base}) is defined as $L_{Gate} - 2L_{OV} - 2L_{Grad}$.

Figure 2b illustrates the relationship between C_1, defined at a specific gate voltage V_1, and the corresponding onset position of accumulation (y_1). Here, C_1 is defined as $C_1 \equiv C_{GG} - \min(C_{GG})$, representing the incremental capacitance due to channel accumulation. When the gate voltage is V_1 ($< V_{ON}$), accumulation begins at position y_1, and the resulting capacitance follows $C_1 = 2{\cdot}W{\cdot}C_{OX}{\cdot}y_1$, where the factor of 2 reflects simultaneous expansion from both the source and drain sides. More specifically, the measured C_{GG} can be decomposed as $C_{GG}(V_G) = C_{para} + C_{OV} + C_{OX}{\cdot}W{\cdot}(y_s + y_d)$, where y_s and y_d denote the accumulation-onset lengths extending from the source and drain sides, respectively. Since min (C_{GG}) corresponds to the gate-voltage-independent components (i.e., min (C_{GG}) = C_{para} + C_{OV} near $V_{G,min}$), the incremental term becomes $C_1 = C_{GG} - \min(C_{GG}) = C_{OX}{\cdot}W{\cdot}(y_s + y_d)$. Under the symmetric expansion assumption $y_s = y_d = y_1$, this directly yields $C_1 = 2{\cdot}W{\cdot}C_{OX}{\cdot}y_1$. In contrast, when C_{GS} or C_{GD} is used instead of C_{GG}, the factor becomes 1, enabling independent extraction of the carrier distribution on either side of the channel. For example, $C_{1,D} \equiv C_{GD} - \min(C_{GD}) = C_{OX}{\cdot}W{\cdot}y_d$ (and similarly $C_{1,S} \equiv C_{GS} - \min(C_{GS}) = C_{OX}{\cdot}W{\cdot}y_s$), because C_{GD} (or C_{GS}) senses only the drain-side (or source-side) accumulation contribution rather than the sum of both sides.

At $V_1 = V_{ON}$, the condition $C_1 = 2{\cdot}C_{OX}{\cdot}W{\cdot}L_{Grad}$ and $y_1 = L_{Grad}$ holds, marking the onset of accumulation in the base channel region with the lowest doping concentration ($L_{Grad} < y_1 < L_{eff} - L_{Grad}$). For $V_1 > V_{ON}$, the base region gradually evolves from weak to strong accumulation, and the simple linear relation $C_1 = 2{\cdot}W{\cdot}C_{OX}{\cdot}y_1$ no longer applies.

Figure 2c shows the relationship between the gate voltage V_1 and the equilibrium carrier concentration n_0 at position y_1. This step converts the spatially mapped local onset-voltage distribution $V_1(y_1)$ (obtained from the $C_1 \leftrightarrow y_1$ relation in Figure 2b) into an equilibrium carrier profile by integrating the accumulation-induced incremental capacitance. Following the standard charge–capacitance relation in gated structures (i.e., $Q = \int C\,dV$), the accumulation-induced gate charge associated with the region that starts accumulating at $y_1$is defined as $Q_{acc}(y_1) = \int_{V_1}^{0} C_1\,(V_G)\,dV_G$ [15, 16]. Here, n_0 is defined as the accumulated charge from $V_G = V_1$ (onset of accumulation) to $V_G = 0$ V and it is expressed as

$$n_0 = \frac{C_{ox}\,(0 - V_1)}{q\,t_{act}} \tag{1}$$

where q is the elementary charge and t_{act} is the IGZO channel thickness. Because $C_1 \equiv C_{GG} - \min(C_{GG})$ removes the gate-voltage-independent components (e.g., parasitic and overlap

2199160x, 2026, 10, Downloaded from https://advanced.onlinelibrary.wiley.com/doi/10.1002/aelm.202500841 by Hanyang University Library, Wiley Online Library on [19/11/2026]. See the Terms and Conditions (https://onlinelibrary.wiley.com/terms-and-conditions) on Wiley Online Library for rules of use; OA articles are governed by the applicable Creative Commons License

contributions) from C_{GG}, the voltage integral $\int_{V_1}^{0} C_1(V_G)\,dV_G$ represents only the accumulation-induced gate charge associated with the channel region that starts accumulating at y_1. Normalizing this charge by q and t_{act} yields $n_0(y_1)$ as a physically meaningful equilibrium electron concentration. Thus, $V_1(y_1)$ describes the spatial distribution of turn-on voltage, whereas $n_0(y_1)$ represents the equilibrium carrier distribution across the channel. Physically, $V_1(y_1)$ can be regarded as the local accumulation-onset (local turn-on) voltage at position y_1, and $n_0(y_1)$ is the corresponding equilibrium electron concentration at $V_G = 0$ V. If $V_1(y_1) > 0$, the integral can yield a negative n_0, indicating that the location remains in a de-accumulated (electron-depleted) state at zero bias; in such cases, we set $n_0(y_1) = 0$ to maintain physical consistency (as described in Figure 2d).

Figure 2d illustrates the procedure for constructing $n_0(y)$ and the corresponding $N_D(y)$. The n_0–y_1 curve near the source is mirrored as $n_0 - (L_{eff} - y_1)$ near the drain, and the two values are combined. In the base channel region ($L_{Grad} < y_1 < L_{eff} - L_{Grad}$), the concentration is set as $n_0(y) = \min(n_0(y))$ to complete the profile (black line). When $V_{ON} > 0$, regions with $V_1(y_1) > 0$ yield negative n_0, indicating depletion at zero bias; in such cases, $n_0(y_1)$ is replaced by zero, giving the corrected profile (red line).

Conversion from $n_0(y)$ to $N_D(y)$ requires correction for equilibrium band-bending. At low N_D, n_0 underestimates N_D, but at higher N_D the difference diminishes, and in accumulation $N_D \approx n_0$. In this work, $N_D(y)$ is defined by offset correction at $\min(n_0)$, ensuring $N_D(y)$ follows the reconstructed $n_0(y)$. The minimum doping concentration (min N_D) is obtained from charge neutrality under flat-band conditions,

$$\min N_D = n_{cFB} + n_{tFB}$$

$$n_{cFB} = N_C \exp\left(-\frac{E_{FB}}{kT}\right)$$

$$n_{tFB} = \int_{E_V}^{E_{FB}} g_A(E)\,f(E)\,dE - \int_{E_{FB}}^{E_C} g_D(E)\,[1 - f(E)]\,dE \qquad (2)$$

where $g_A(E)$, $g_D(E)$, E_{FB}, and V_{FB} were extracted by the monochromatic photonic capacitance– voltage (MPCV) method [17], and $N_C \approx 5.0 \times 10^{18}$ cm^{-3} was adopted from the literature [17]. For depletion-mode devices ($V_{ON} < V_{FB}$), min N_D is alternatively defined as

$$\min N_D = \frac{C_{ox}}{qt_s}\,(V_{FB} - V_{ON}) \qquad (3)$$

2.2 | Applicability and Limitations

The proposed C–V-based profiling method is applicable to accumulation-mode TFTs in which the effective accumulation area changes monotonically with V_G within the analysis window ($V_{G,min} \le V_G \le V_{ON}$) and the incremental capacitance C_1 is dominantly governed by accumulation charge. Careful interpretation may be required when (i) strong frequency dispersion or hysteresis indicates significant trap response, (ii) parasitic/overlap components are not sufficiently removed (inaccurate C_{para} correction), (iii) large series resistance distorts the measured C–V at high frequency, or (iv) in extremely short-channel devices, the accumulation-induced incremental capacitance within the analysis window can close to the resolution limit (often comparable to parasitic components and measurement noise), which limits reliable y_1 mapping and thus constrains the extraction of $N_D(y)$. In addition, the extracted $N_D(y)$ represents an electrically effective doping (effective charge density) associated with V_O/H-related donor and thus may not be interpreted as a direct one-to-one chemical concentration profile without complementary material analyses.

3 | Results and Discussion

3.1 | Experimental Verification via TLM Comparison

To validate the proposed C–V-based lateral doping profile extraction method, we rely on experimental results obtained from L-split self-aligned top-gate coplanar a-IGZO TFTs. This verification framework is constructed using directly measured electrical characteristics, enabling a transparent comparison between our proposed method and an established experimental technique, namely the transfer length method (TLM). Figure 3 presents the raw experimental data utilized for this validation. Figure 3a illustrates the measured transfer characteristics (I_{DS}–V_{GS}) of the L-split SATG a-IGZO TFTs, configured with a fixed channel width of 50 μm and various channel lengths (4.5, 5.5, 6.5, 7.5, 8.5, 11.5, 15.5, and 40 μm). The gate voltage (V_{GS}) was swept from −15 V to +15 V, and the transfer curves were measured under two drain bias conditions: V_{DS} = 0.1and 10 V. These datasets serve as the foundation for the subsequent TLM-based extraction. For completeness, the initial device parameters for each channel length—including the threshold voltage (V_T), subthreshold swing (SS), field-effect mobility (μ_{FE}), turn-on voltage (V_{ON}), and DIBL factor—are summarized in the Supporting Information (Figure S1). Figure 3b displays the measured C–V characteristics of the corresponding L-split devices under identical W/L conditions. The gate voltage was swept from −20 V to +20 V, and the individual gate capacitances (C_{GG}, C_{GD}, and C_{GS}) were obtained after de-embedding the parasitic capacitance (C_{para}). All C–V measurements were performed at a frequency of 100 kHz. This specific frequency was chosen as an optimal compromise between low-frequency measurement variability and high-frequency roll-off effects. At excessively low frequencies, the capacitive current diminishes, leading to increased measurement noise; conversely, at excessively high frequencies, the measured capacitance can be artificially suppressed due to distributed RC-related limitations and the reduced AC response of trap states. The frequency-dependent C–V characteristics, measured across a range of 10 kHz to 1 MHz, are provided in the Supporting Information (Figure S2), which further justifies the selection of 100 kHz for our primary analysis.

Figure 4 illustrates the lateral-doping profile $N_D(y)$ model for self-aligned top-gate (SATG) IGZO TFTs. This Gaussian-based profile model is used solely as a compact representation to fit

2199160x, 2026, 10, Downloaded from https://advanced.onlinelibrary.wiley.com/doi/10.1002/aelm.202500841 by Hanyang University Library, Wiley Online Library on [19/11/2026]. See the Terms and Conditions (https://onlinelibrary.wiley.com/terms-and-conditions) on Wiley Online Library for rules of use; OA articles are governed by the applicable Creative Commons License

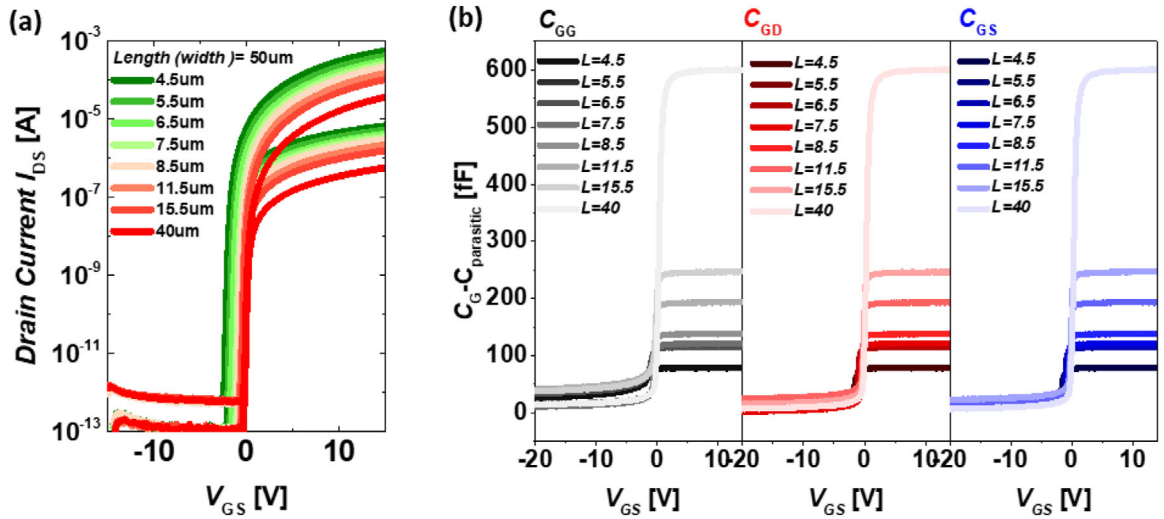

FIGURE 3 | a) Measured transfer characteristics (I–V) of the L-split SATG a-IGZO TFTs (W = 50 μm (fixed), L = 4.5–40 μm) used for the TLM analysis. b) Gate capacitance characteristics (C_{GG}, C_{GD}, and C_{GS}) of the corresponding devices used for the proposed C–V-based extraction, plotted after de-embedding of parasitic capacitance.

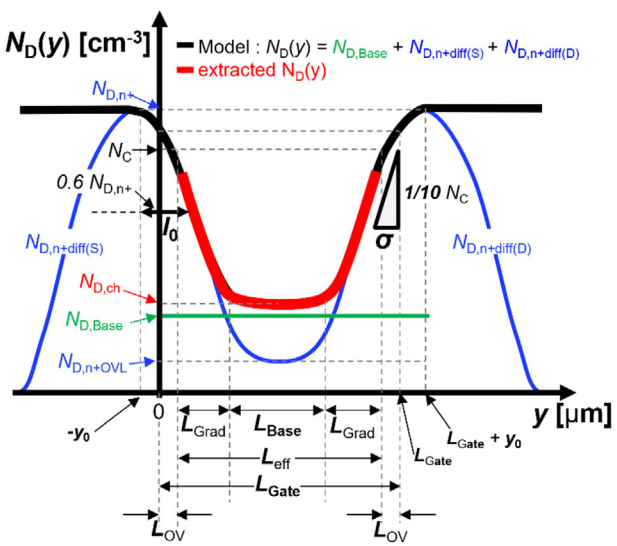

FIGURE 4 | Gaussian-modeled $N_D(y)$ profile for SATG IGZO TFTs. $N_D(y)$ is expressed as the sum of $N_{D,Base}$ and diffusion components from n^+ regions. Main parameters include $N_{D,Base}$, $N_{D,n+}$, y_0, and l_0, which describe base doping, peak doping, offset, and diffusion length, respectively.

the experimentally extracted $N_D(y)$ profiles (from the C–V based method or TLM method) and the model parameters reported here are experimental fitting parameters. The doping concentration in the channel is expressed as the sum of the base doping concentration ($N_{D,Base}$) and the contributions diffused from the source and drain n^+ regions, as defined in Equation (4):

$$N_D(y) = N_{D,\text{Base}} + N_{D,n^+\text{diff(S)}} + N_{D,n^+\text{diff(D)}} = N_{D,\text{Base}} + N_{D,n^+} \exp \times \left[-\frac{1}{2}\left(\frac{y+y_0}{l_0}\right)^2\right] + N_{D,n^+} \exp \left[-\frac{1}{2}\left(\frac{y-(L_{\text{Gate}}+y_0)}{l_0}\right)^2\right] \quad (4)$$

here, $N_{D,n+}$ is the peak doping concentration in the n^+ regions, y_0 is the Gaussian peak offset from the gate edge (y = 0), and l_0 is the characteristic diffusion length, which is proportional to $\sqrt{Dt}$ with diffusivity D and process time t [18]. In addition, $N_{D,ch}$, L_{OV}, and σ are defined to better describe the effective channel doping and electrical characteristics. Typically, dopant profiles are expressed with an error function for continuously supplied sources and a Gaussian function for limited dopant amounts [19], but the devices studied here were accurately represented by the Gaussian-based model.

At the channel center ($y = L_{Gate}/2$), the doping concentration $N_{D,ch}$ corresponds to the minimum of $N_D(y)$ and is expressed as

$$N_{D,ch} = \min N_D = N_{D,\text{base}} + N_{D,n^+\text{OVL}} = N_{D,\text{base}} + 2N_{D,n^+} \exp\left[-\frac{1}{2}\left(\frac{L_{\text{gate}}/2+y_0}{l_0}\right)^2\right] \quad (5)$$

In Equation (5), $N_{D,ch}$ represents the actual center-channel doping, whereas $N_{D,n^+,OVL}$ denotes the overlap contribution from the two n^+ regions. The overlap length (L_{OV}) is defined where $N_D \geq N_C$, the effective channel length is given as $L_{eff} = L_{Gate} - 2L_{OV}$, and the doping gradient σ is defined as the distance over which N_D decreases by one order of magnitude at $y = y_0 + L_{OV}$.

Figure 5 presents the extraction results of the proposed C–V-based profiling method and demonstrates its superiority by directly comparing it with the conventional TLM method. First, Figure 5a displays the extracted lateral doping profile ($N_D(y)$) data points and the corresponding Gaussian model fits for various channel lengths (L = 4.5 to 40 μm) using the C–V-based method. The extracted profiles clearly resolve the highly doped source/drain (S/D) extension regions, the transitional gradient regions, and the uniform base channel region. More importantly, the proposed method successfully captures the

2199160x, 2026, 10, Downloaded from https://advanced.onlinelibrary.wiley.com/doi/10.1002/aelm.202500841 by Hanyang University Library, Wiley Online Library on [19/11/2026]. See the Terms and Conditions (https://onlinelibrary.wiley.com/terms-and-conditions) on Wiley Online Library for rules of use; OA articles are governed by the applicable Creative Commons License

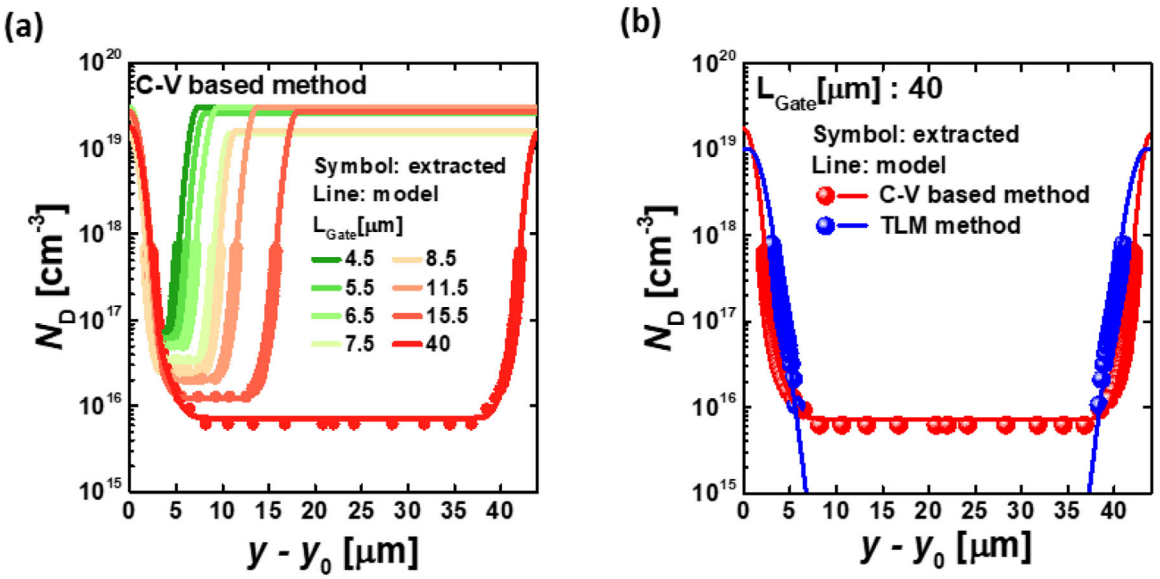

FIGURE 5 | a) Extracted lateral doping profiles ($N_D(y)$) and corresponding model fits for all channel lengths (L) using the proposed C–V-based method. b) Comparison of the extracted $N_D(y)$ profiles and the models obtained from the C–V-based method and the TLM method at L = 40 μm.

channel-length-dependent behavior, where the lateral diffusion of S/D dopants increasingly overlaps in shorter channels, thereby elevating the effective doping concentration at the channel center. Figure 5b directly compares the $N_D(y)$ profiles obtained from the proposed C–V-based method and the conventional TLM method for the L = 40 μm device. (For completeness and reproducibility, detailed TLM experimental procedures—including ΔL extraction, width-normalized R_{ext} analysis, and intermediate steps for deriving the lateral carrier distribution—are thoroughly provided in the Supporting Information, Figure S3) This comparison highlights the significant advantages of the C–V-based method over the TLM approach. Because TLM-based extraction relies on channel-length-dependent resistance analysis, it inherently reflects lumped, averaged characteristics across the channel. Consequently, its spatial resolution is strictly limited, particularly in the transitional gradient regions and low-doping base regions, leading to a loss of precise local doping variations. In contrast, the proposed C–V-based method directly tracks the displacement of the accumulation boundary in response to the gate bias. This mechanism allows for a much more spatially fine, continuous, and highly resolved reconstruction of the doping profile, even within the steep gradient regions.

The detailed fitting parameters corresponding to the lateral doping profiles presented in Figure 5 are summarized in Table 2. Each parameter listed in the table was derived by fitting the experimentally extracted $N_D(y)$ to the lateral profile model defined earlier in Figure 4. The base channel length (L_{Base}) systematically decreases as the channel length scales down. This quantitatively reflects that the dominant influence of the highly doped source/drain (S/D) extension regions on the effective channel area gradually increases for shorter physical channel lengths. Simultaneously, the gradient length (L_{Grad}) and doping gradient (σ) also exhibit variations, suggesting that the doping transition characteristics between the highly doped S/D extensions and the base channel are finely modulated by the channel length. Most importantly, the effective doping concentration at the channel center ($N_{D,ch}$) sharply increases as the channel length decreases. This clearly demonstrates that the overlap effect of lateral dopant diffusion from the S/D is maximized in short channels, whereas its impact becomes relatively marginal in long channels. Meanwhile, the overlap length (L_{OV}) generally maintains a small value close to zero, which aligns well with the characteristics of the Self-Aligned Top-Gate (SATG) structure used in this study. The small negative L_{OV} values observed in some devices can be attributed to a microscopic offset or under-diffusion occurring during the n^+ doping region formation (e.g., plasma treatment and etching processes).

For comparative validation, the parameters derived from the conventional TLM analysis are also presented in the last column of Table 2. Notably, the doping gradient (σ) extracted from the TLM method is 0.32 μm/decade, which is significantly overestimated compared to the proposed C–V-based method (0.12 – 0.24 μm/decade). This overestimation occurs because the TLM analysis relies on macroscopic, lumped resistance characteristics across the entire channel, thereby lacking the spatial resolution required in the transition region where the doping concentration changes gradually. Consequently, it misinterprets the profile as being more widely spread than it actually is. These results strongly support that the proposed C–V-based profiling method is superior and more reliable than the conventional TLM approach in accurately capturing microscopic, localized doping variations.

3.2 | Experimental ND Profiling and Short Channel Effect Analysis

Figure 6 illustrates the procedure for predicting V_T (V_{ON}) roll-off using the proposed C–V based profiling method. Figure 5a shows the reconstructed $N_D(y)$ distribution, highlighting both the dif-

2199160x, 2026, 10, Downloaded from https://advanced.onlinelibrary.wiley.com/doi/10.1002/aelm.202500841 by Hanyang University Library, Wiley Online Library on [19/11/2026]. See the Terms and Conditions (https://onlinelibrary.wiley.com/terms-and-conditions) on Wiley Online Library for rules of use; OA articles are governed by the applicable Creative Commons License

TABLE 2 | Summary of extracted lateral doping profile parameters.

Parameters (units)	L4.5	L5.5	L6.5	L7.5	L8.5	L11.5	L15.5	L40	TLM
$L_{effective}$ (μm)	4.3	4.7	5.7	8.2	8.9	10.4	14.7	40.7	40
L_{OV} (μm)	0.1	0.4	0.4	−0.4	−0.2	0.5	0.4	−0.4	0.0
L_{GRAD} (μm)	1.6	1.5	1.8	1.5	2.2	3.2	4.0	6.0	—
L_{BASE} (μm)	1.2	1.8	2.1	5.2	4.5	4.1	6.6	28.6	—
σ (μm/decade)	0.16	0.15	0.18	0.12	0.17	0.17	0.24	0.13	0.32
$y_{0,1}$ (μm)	−1.1	−0.7	−0.8	−1.9	−1.7	−0.9	−1.1	−1.6	−1.5
$l_{0,1}$ (μm)	0.35	0.27	0.32	0.40	0.39	0.40	0.42	0.40	0.61
$N_{D,n+,1}$ (10^{19} cm^{-3})	2.03	3.00	3.00	2.94	2.77	2.67	2.32	1.56	1.00
$y_{0,2}$ (μm)	−0.8	0.0	0.0	0.0	−0.6	0.0	−0.7	−1.0	−0.4
$l_{0,2}$ (μm)	0.31	0.30	0.36	0.38	0.41	0.61	0.81	0.87	0.78
$N_{D,n+,2}$ (10^{17} cm^{-3})	0.00	4.33	3.46	0.77	4.91	1.31	1.22	0.84	2.11
$N_{D,ch}$ (10^{16} cm^{-3})	7.3	6.97	5.23	3.38	2.73	2.1	1.28	0.62	—
$N_{D,base}$ (10^{16} cm^{-3})	7.26	6.97	5.22	3.38	2.73	2.09	1.28	0.62	—
$N_{D,ch,\ n+\ OVL}$ (10^{15} cm^{-3})	0.43	0.07	0.06	0.00	0.00	0.01	0.00	0.00	—

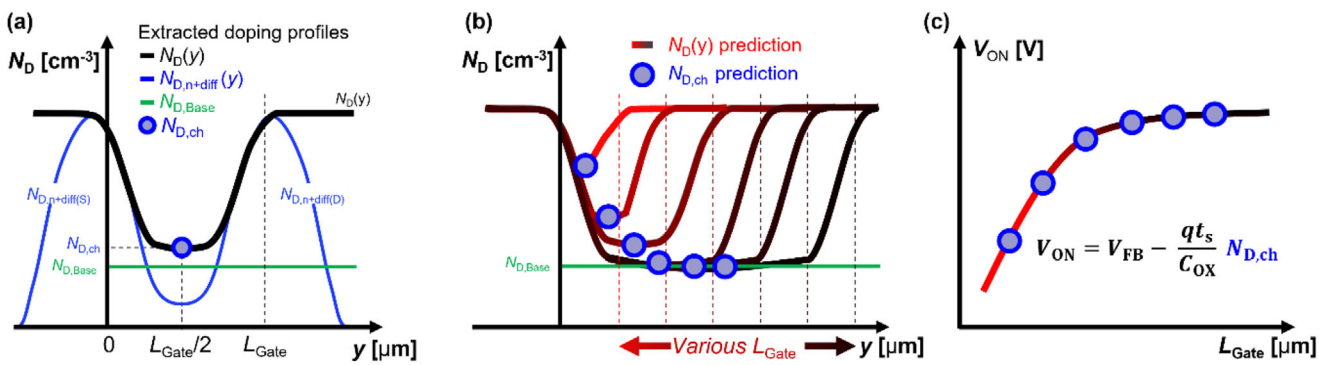

FIGURE 6 | Conceptual prediction of $V_T(V_{ON})$ roll-off from extracted $N_D(y)$. a) Modeled $N_D(y)$ distribution with $N_{D,Base}$ and $N_{D,n+\ diff}$. b) Channel-length dependence of $N_{D,ch}$. c) Final $V_T(V_{ON})$ roll-off curve predicted by its conversion into V_{ON} using Equation (6). Shorter channels yield higher $N_{D,ch}$ and accelerated V_{ON} roll-off.

fused doping component from the n^+ regions [$N_{D,n+\ diff}(y)$] and the baseline concentration $N_{D,Base}$. In Figure 6b, the channel length (L_{Gate}) is varied to calculate the corresponding channel-center doping concentration $N_{D,ch}$ using Equation (5), and subsequently, the turn-on voltage V_{ON} is derived according to Equation (6) [20]:

$$V_{ON} = V_{FB} - \frac{qt_s}{C_{OX}} N_{D,ch} \tag{6}$$

As L_{Gate} decreases, $N_{D,ch}$ increases, leading to a rapid reduction in V_{ON} and thereby manifesting as V_T (V_{ON}) roll-off. The difference between V_{ON} and V_T is primarily governed by variations in E_{FB} within the density of states (DoS). If E_{FB} remains nearly constant with channel length, V_T and V_{ON} differ only by a constant offset, allowing the predicted V_{ON} roll-off to closely represent the actual V_T roll-off. Figure 5c presents the final V_T (or V_{ON}) roll-off curve predicted through this procedure.

In this section, the extracted $N_D(y)$ profiles as a function of channel length are analyzed using the proposed method and discussed in relation to short-channel effects (SCE). Figure 7a schematically illustrates that as the channel length decreases, the diffused $N_{D,diff}$ component from the n^+ regions increasingly overlaps at the channel center, sharply raising $N_{D,ch}$. The fabrication process is described in Section 2. Figure 7b compares the extracted $N_D(y)$ profiles for devices with W = 50 μm and L in a range between 4.5 and 40 μm, fitted with the proposed model. The diffused doping concentration ($N_{D,n+\ diff}$) is well represented by two Gaussian components, $N_{D1}(y)$ and $N_{D2}(y)$. Although the exact physical origin is not fully clarified, they are most likely associated with different dopant species; $N_{D1}(y)$ is presumed to be related to V_O and $N_{D2}(y)$ to hydrogen [21]. As shown in Figure 7c, N_{D1} ($\approx 2 \times 10^{17}$–10^{19} cm^{-3}) remains nearly invariant with channel length, suggesting a steep doping gradient that is less sensitive to overlap. By contrast, Figure 7d shows that N_{D2} ($\approx 10^{15}$–2×10^{17} cm^{-3}) decreases in L_{Grad} while $N_{D,ch}$ increases as the channel length shortens. This reflects a more gradual gradient, where dopant diffusion from the source and drain sides overlaps at the channel center and accumulates, thereby raising N_D.

2199160x, 2026, 10, Downloaded from https://advanced.onlinelibrary.wiley.com/doi/10.1002/aelm.202500841 by Hanyang University Library, Wiley Online Library on [19/11/2026]. See the Terms and Conditions (https://onlinelibrary.wiley.com/terms-and-conditions) on Wiley Online Library for rules of use; OA articles are governed by the applicable Creative Commons License

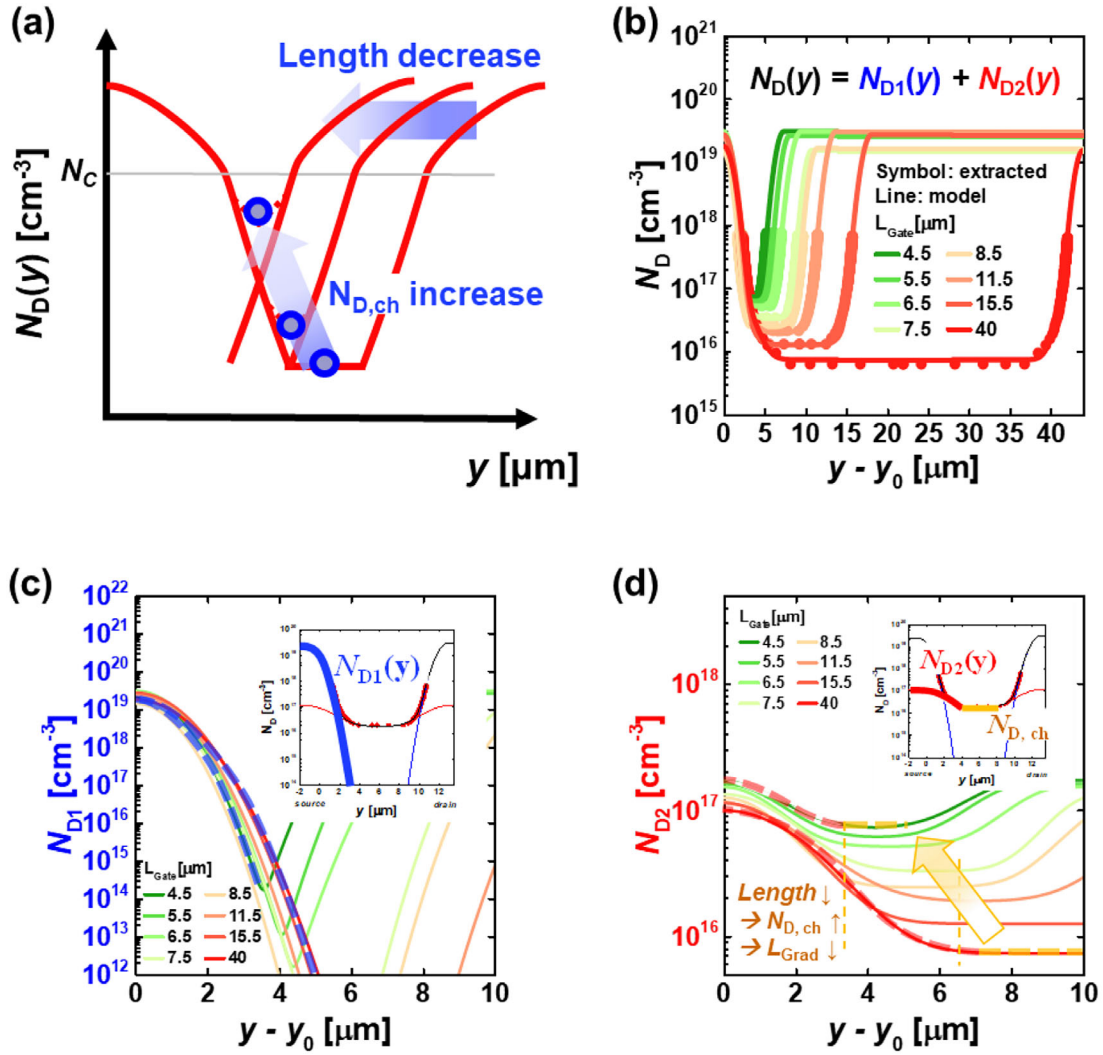

FIGURE 7 | Experimental analysis of extracted $N_D(y)$ profiles. a) Schematic of n^+ diffusion overlap at short channel lengths. b) Extracted $N_D(y)$ for L = 4.5–40 μm, fitted by double Gaussian model (N_{D1}, N_{D2}). c) High-concentration Gaussian component (N_{D1}) showing steep, length-independent behavior. d) Low-concentration component (N_{D2}) exhibiting gradual gradient, with L_{Grad} decrease and $N_{D,ch}$ increase at shorter channels.

Figure 8a compares the predicted N_D profiles of short-channel devices (L = 4.5 μm), obtained from long-channel N_D profiles (L = 40 μm) using either the TLM or the proposed C–V method, with the N_D profiles directly extracted from short-channel devices by C–V measurements. Because the TLM method provides only an averaged N_D profile without accounting for channel-length-dependent variations, its prediction at L = 4.5 μm deviates significantly from the measured result. On the other hand, the C–V method directly resolves the variation of $N_{D,ch}$ at both long and short channels, demonstrating its ability to capture length-dependent doping distributions. Figure 8c further compares the predicted $V_T(V_{ON})$ roll-off characteristics with experimental results. Both TLM- and C–V-based predictions derived from L = 40 μm data accumulate errors as L decreases. However, the C–V method allows regression of the base doping variation with channel length [$\Delta N_{D,Base}(L)$], which can be incorporated into the V_{ON} calculation, as derived in Equation (7):

$$V_{ON} = V_{FB} - \frac{qt_s\left(\min N_D + \Delta N_{D,Base}(L)\right)}{C_{OX}} \quad (7)$$

This correction yields predictions that closely track the experimentally observed $V_T(V_{ON})$ roll-off, highlighting the superior predictive accuracy of the C–V approach.

In addition, as the channel length decreases, L_{Base} shrinks and the high-doping regions extend closer to the channel center, making the central potential increasingly sensitive to DIBL [22]. This results in enhanced DIBL, which follows the same trend as $V_T(V_{ON})$ roll-off in Figure 8c. The correlation arises because diffused dopants from the n^+ regions ($N_{D,ch,n+\ OVL}$) contribute simultaneously to $V_T(V_{ON})$ roll-off and to modulation of the carrier distribution (n_e) through channel potential variations [23]. In summary, the proposed C–V method uniquely provides direct access to channel-length-dependent N_D profiles that cannot be obtained with the TLM approach. This capability enables accurate prediction of both $V_T(V_{ON})$ roll-off and DIBL across a wide range of channel lengths for SATG TFTs, including the short-channel regime, offering a powerful tool for oxide TFT scaling. Whereas spatially resolved material characterizations (e.g., XPS/EDS/SIMS) could provide complementary evidence for the distribution of diffused species near the S/D extensions,

2199160x, 2026, 10, Downloaded from https://advanced.onlinelibrary.wiley.com/doi/10.1002/aelm.202500841 by Hanyang University Library, Wiley Online Library on [19/11/2026]. See the Terms and Conditions (https://onlinelibrary.wiley.com/terms-and-conditions) on Wiley Online Library for rules of use; OA articles are governed by the applicable Creative Commons License

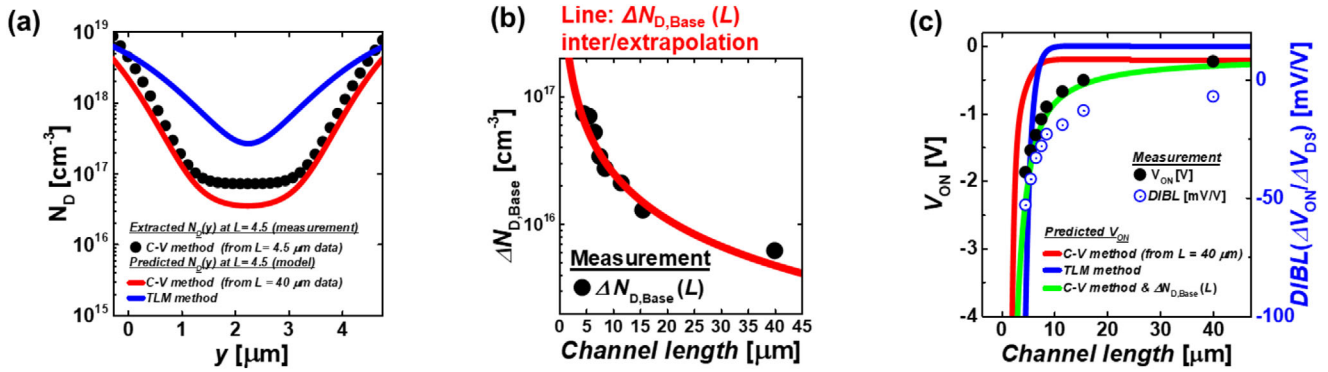

FIGURE 8 | Comparison of experimental $N_D(y)$ and V_T roll-off predictions. a) Short-channel (L = 4.5 μm) $N_D(y)$ profiles predicted from long-channel (L = 40 μm) data using the TLM and C–V methods, compared with direct C–V measurements. b) Extraction of the channel-length-dependent base doping variation $\Delta N_{D,Base}(L)$ from experimental data for use in V_{ON} correction. c) V_{ON} roll-off comparison: black dots indicate measured values, red solid line shows C–V predictions, blue solid line shows TLM predictions, and green solid line shows C–V predictions corrected with $\Delta N_{D,Base}(L)$, which closely match to experiment results. Measured DIBL factors are also plotted as blue dots.

such analyses typically require destructive sample preparation and dedicated test structures. Due to the constraints and limited access to the devices, these direct characterizations are beyond the scope of the present study and will be investigated in future work.

4 | Conclusions

In this work, we proposed a C–V-based analysis technique to precisely extract the lateral doping profile $N_D(y)$ in self-aligned top-gate coplanar a-IGZO TFTs. By mapping the incremental gate capacitance to the accumulation-onset position and converting the local onset-voltage distribution into an equilibrium carrier profile, the method reconstructs $N_D(y)$ and extracts key parameters (L_{OV}, L_{Grad}, L_{Base}, $N_{D,Base}$, and $N_{D,ch}$) directly from measurements. The validity of the approach was established using a fully experimental verification framework: L-split devices were analyzed by both the proposed C–V method and a TLM-based method, and the extracted profiles were further used to quantitatively predict $V_T(V_{ON})$ roll-off and DIBL over channel lengths of 4.5–40 μm. The results show that S/D diffusion overlap increases $N_{D,ch}$ in short channels, which simultaneously accelerates $V_T(V_{ON})$ roll-off and enhances DIBL, providing a direct link between lateral dopant diffusion (V_O/H-related donor-like states) and SCEs. Overall, the proposed C–V profiling framework offers a practical diagnostic and design tool for suppressing SCEs in BEOL-compatible low-power oxide electronics and next-generation display driver circuits.

Acknowledgements

This work was supported in part by the LG Display, in part by the National Research Foundation of Korea (NRF) funded by the Korean Government (MSIT) under Grant RS-2023-00208661 and RS-2024-00409492, in part by the Tech Incubator Program for Startup (TIPS) funded by the Korea government under Grant 00321794, and in part by the 2023 research fund of Kookmin University in Korea. The EDA tool was supported by the IC Design Education Center (IDEC), Korea.

Conflicts of Interest

The authors declare no conflict of interest.

Data Availability Statement

The data that support the findings of this study are available from the corresponding author upon reasonable request.

References

1. K. Nomura, H. Ohta, A. Takagi, T. Kamiya, M. Hirano, and H. Hosono, "Room-Temperature Fabrication of Transparent Flexible Thin-Film Transistors Using Amorphous Oxide Semiconductors," *Nature* 432 (2004): 488.

2. W. Nam, J. Shim, H. Shin, et al., "21.2: Distinguished Paper: 55-Inch OLED TV Using InGaZnO TFTs with WRGB Pixel Design," *SID Symposium Digest of Technical Papers* 44 (2013): 243–246, https://doi.org/10.1002/j.2168-0159.2013.tb06190.x.

3. J. Y. Noh, D. M. Han, W. C. Jeong, J. W. Kim, and S. Y. Cha, "21-1: Development of 55″ 4K UHD OLED TV Employing the Internal Gate IC with High Reliability and Short Channel IGZO TFTs," *SID Symposium Digest of Technical Papers* 48 (2017): 288–290, https://doi.org/10.1002/sdtp.11605.

4. H.-J. Shin, S.-H. Choi, S.-J. Kim, et al., "76-2: Distinguished Paper: a High-Image-Quality OLED Display with Motion Blur Reduction for Ultra-High Resolution and Premium TVs," *SID Symposium Digest of Technical Papers* 51 (2020): 1131–1134, https://doi.org/10.1002/sdtp.14075.

5. T.-K. Chang, C.-W. Lin, and S. Chang, "39-3: Invited Paper: LTPO TFT Technology for AMOLEDs †," *SID Symposium Digest of Technical Papers* 50 (2019): 545–548, https://doi.org/10.1002/sdtp.12978.

6. U.-J. Chung, S.-C. Choi, S. Y. Noh, et al., "15-1: Invited Paper: Manufacturing Technology of LTPO TFT," *SID Symposium Digest of Technical Papers* 51 (2020): 192–195, https://doi.org/10.1002/sdtp.13835.

7. J. Park, S. Go, W. Chae, et al., "Floating Body Effect in Indium–gallium–zinc–oxide (IGZO) Thin-film Transistor (TFT)," *Scientific Reports* 14 (2024): 10067, https://doi.org/10.1038/s41598-024-60288-z.

8. D. Kim, D. Lee, W. Kim, et al., "Cation Composition Ratio and Channel Length Effects on Bias Stress Instability in Amorphous InGaZnO Back-end-of-line Field-effect Transistors," *Scientific Reports* 14 (2024): 30873, https://doi.org/10.1038/s41598-024-81556-y.

9. G. J. Hu, C. Chang, and Y.-T. Chia, "Gate-voltage-dependent Effective Channel Length and Series Resistance of LDD MOSFET's," *IEEE Trans-*

2199160x, 2026, 10, Downloaded from https://advanced.onlinelibrary.wiley.com/doi/10.1002/aelm.202500841 by Hanyang University Library, Wiley Online Library on [19/11/2026]. See the Terms and Conditions (https://onlinelibrary.wiley.com/terms-and-conditions) on Wiley Online Library for rules of use; OA articles are governed by the applicable Creative Commons License

actions on Electron Devices 34 (1987): 2469–2475, https://doi.org/10.1109/T-ED.1987.23337.

10. J. Zhang, Z. Lin, Z. Zhang, et al., "Back-End-of-Line-Compatible Scaled InGaZnO Transistors by Atomic Layer Deposition," *IEEE Transactions on Electron Devices* 70 (2023): 6651–6657, https://doi.org/10.1109/TED.2023.3312357.

11. S.-Y. Hong, H.-J. Kim, D.-H. Kim, et al., "Study on the Lateral Carrier Diffusion and Source-Drain Series Resistance in Self-Aligned Top-Gate Coplanar InGaZnO Thin-Film Transistors," *Scientific Reports* 9 (2019): 6588, https://doi.org/10.1038/s41598-019-43186-7.

12. S. H. Kim, M. Kim, J. H. Lee, et al., "Optimizing Length Scalability of InGaZnO Thin-Film Transistors through Lateral Carrier Profile Engineering and Negative Δ L Extension Structure," *Advanced Electronic Materials* 10 (2024): 2400012, https://doi.org/10.1002/aelm.202400012.

13. K. Imanishi, T. Matsuda, and M. Kimura, "Analysis of Carrier Mobility in Amorphous Metal-Oxide Semiconductor Thin-Film Transistor Using Hall Effect," *IEEE Electron Device Letters* 41 (2020): 1025.

14. L. Liu, Z. Mei, A. Tang, et al., "Oxygen Vacancies: The Origin of *n*-type Conductivity in ZnO," *Physical Review B* 93 (2016): 235305.

15. E. H. Nicollian and J. R. Brews, *MOS (Metal Oxide Semiconductor) Physics and Technology*, John Wiley & Sons, New York 2002.

16. D. K. Schroder, *Semiconductor Material and Device Characterization*. (John Wiley & Sons, 2015).

17. H. Bae, H. Choi, S. Jun, et al., "Single-Scan Monochromatic Photonic Capacitance-Voltage Technique for Extraction of Subgap DOS Over the Bandgap in Amorphous Semiconductor TFTs," *IEEE Electron Device Letters* 34 (2013): 1524.

18. S. J. Myoung, C. I. Ryoo, C. Kim, et al., "Thermal Process and Dopant Diffusion Model of a-InGaZnO TFTs for VT Prediction Using Lateral Carrier Density Profiling Technique," *IEEE Electron Device Letters* 44 (2023): 630.

19. J. D. Plummer, M. D. Deal, and P. B. Griffin, *Silicon VLSI Technology: Fundamentals, Practice and Modeling* (Prentice Hall, Upper Saddle River, NJ, USA, 2000).

20. D. Hong, G. Yerubandi, H. Q. Chiang, M. C. Spiegelberg, and J. F. Wager, "Electrical Modeling of Thin-Film Transistors," *Critical Reviews in Solid State and Materials Sciences* 33 (2008): 101.

21. H. Y. Noh, W.-G. Lee, G. R. Haripriya, et al., "Hydrogen Diffusion and Its Electrical Properties Variation as a Function of the IGZO Stacking Structure," *Scientific Reports* 12 (2022): 19816, https://doi.org/10.1038/s41598-022-24212-7.

22. T. J. Yang, J.-H. Kim, C. I. Ryoo, et al., "Analysis of Drain-Induced Barrier Lowering in InGaZnO Thin-Film Transistors," *IEEE Transactions on Electron Devices* 70 (2023): 121.

23. J. A. del Alamo, *Integrated Microelectronic Devices: Physics and Modeling* (Pearson, New York, USA 2018).

Supporting Information

Additional supporting information can be found online in the Supporting Information section.

Supporting File: aelm70384-sup-0001-SuppMat.docx.

2199160x, 2026, 10, Downloaded from https://advanced.onlinelibrary.wiley.com/doi/10.1002/aelm.202500841 by Hanyang University Library, Wiley Online Library on [19/11/2026]. See the Terms and Conditions (https://onlinelibrary.wiley.com/terms-and-conditions) on Wiley Online Library for rules of use; OA articles are governed by the applicable Creative Commons License